Chapter 2
Theory: Bond–Band–Barrier (3B) Correlation

- *Chemical bond, energy band, and surface potential are closely correlated.*
- *O, N, and C hybridize their sp orbit upon reacting with atoms in any phase to create tetrahedral bonding orbits.*
- *Non-bonding lone electron pairs and bonding shares electron pairs occupy the orbits. The number of lone pairs follows the (4−n) rule with n being valance value.*
- *The lone pair polarizes its neighboring atoms to form dipoles.*
- *Bond and non-bond formation creates four DOS features in the valence band, i.e., bonding pairs, non-bonding lone pairs, holes, and antibonding dipole states.*
- *Bond formation corrugates the surfaces with subjective production of missing-row vacancies.*

2.1 Basics

2.1.1 Regular Bonds: Interatomic Potential and Electron Configuration

The covalent, ionic, and metallic bonds are the most popular kinds of interatomic interaction [1]. These regular bonds are realized through valence charge sharing, either locally by neighboring atoms in the ionic and covalently bonded systems or delocally by all atoms of the entire body of a metal [1, 2]. The energies of the regular bonds are several electron volts (eV) in magnitude at equilibrium. The nearest distance between atoms and ions at equilibrium corresponds to the bond length. For example, Na is interacted with metallic bond and a cohesive energy of 1.1 eV per atom, which determines the Na to be ductile and electrically and thermally conductive. NaCl is an ideal specimen of ionic bond with a cohesive energy of 3.28 eV/atom, which makes NaCl harder, having high melting point and soluble in polar liquids such as water. Diamond being an ideal example of covalent

C. Q. Sun, *Relaxation of the Chemical Bond*, Springer Series in Chemical Physics 108, DOI: 10.1007/978-981-4585-21-7_2,

bond with cohesive energy of 7.4 eV per atom is so far the hardest natural material with high melting point of 3,800 K; diamond is insoluble in nearly all solvents. The polar covalent bond, in the form between the covalent and the ionic, exists in most alloys or compounds. The electronegativity difference between the constituent elements of the specimen dictates the nature of the bond or the way of charge sharing.

The interatomic potentials for these stronger interactions dominate the atomic cohesive energy, the Hamiltonian and the band structure, dispersion relations, the allowed density of states (DOS) of the valence band and below, and the effective mass and group velocity of charges in various bands as well. At equilibrium, the coordinates of a pairing potential correspond to the bond length and bond energy (d, E_b) that determine the binding energy density, E_b/d^3. The product of the number of bonds (z) of an atom and the cohesive energy per bond is the atomic cohesive energy (z_bE_b). All the detectable quantities of the bulk materials, such as the critical temperature for crystal structural phase transition, electronic and optical properties, hardness, elasticity, and melting point, are all closely related to the bond nature, order, length, and energy represented by m, z, d, and E_b, or their combinations such as the cohesive energy, energy density, and lattice vibration frequency. The cohesive energy determines the thermal stability; the binding energy density determines the elasticity and mechanical strength. Quantum approximations could describe these regular bonds and their functionalities because of their periodically ordered homogeneity and uniformity.

2.1.2 Chemisorption Bonding Environment

Patterns of crystallographic and morphologic observations of the chemisorbed surfaces depend on the scale and geometry of the surface lattice and the difference in electronegativity between the guest and the host.

Figure 2.1 illustrates the typical coordination environment of the low-index fcc and hcp surfaces. Host atoms are arranged at sites between the first two planes of the fcc(001), (110), (111), and the hcp($10\bar{1}0$), (0001) surfaces regularly. The C_{4v}, $C_{3v,}$ and C_{2v} point-group symmetries apply to the unit cells. The shortest atomic separation (atomic diameter) is a. These structures represent the majority of coordination environments so far documented. Table 2.1 compares the lattice geometry of the unit cells.

In the fcc(001) surface unit cell (see Fig. 2.1a), five atoms surrounding the C_{4v} hollow site form an upside-down pyramid. The atomic structures of the fcc(111) and the hcp(0001) surfaces in Fig. 2.1b are the same in the top two atomic planes where atoms arrange in the same *AB* order. Atoms surrounding the hcp(0001) hollow (indicated I) site form a tetrahedron, while atoms surrounding the fcc(111) hollow (indicated II) site cannot because there is no atom in the second layer underneath.

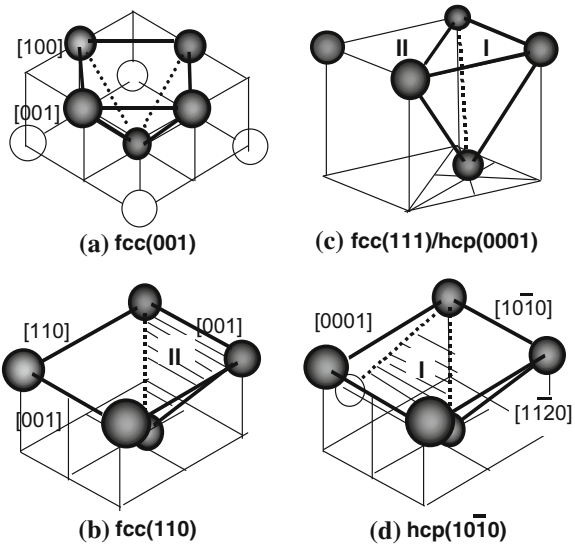

Fig. 2.1 Possible coordination environment for atomic chemisorption. **a** Atoms surrounding the fcc(001) fourfold (C_{4v}) hollow site form an upside-down pyramid. **b** On the fcc(111) and hcp(0001) surfaces, there are two types of threefold (C_{3v}) hollow sites. Atoms surrounding the hcp(0001) hollow (*I*) form a tetrahedron. No atom exists in the substrate second layer below the fcc(111) hollow site (*II*). **c** The fcc(110) and its analog. **d** hcp(10$\bar{1}$0) surfaces possess alternate hcp(0001) (*I*) and fcc(111) (*II*) facet sites along the close-packed direction (reprinted with permission from [3])

Table 2.1 Comparison of the lattice geometry of the unit cells of various surfaces (unit in atomic diameter, *a*) (reprinted with permission from [3])

	a_1	a_2	a_3 (layer spacing)
fcc(001)	1	1	$1/\sqrt{2}$
fcc(110)	1	$\sqrt{2}$	1/2
fcc(111)	1	1	0.6934
hcp(10$\bar{1}$0)	1	1.747	0.2887
hcp(0001)	1	1	0.8735

Atoms surrounding the fcc(110) and the hcp(10$\bar{1}$0) hollow sites, in Fig. 2.1c, d, form a rectangular pyramid of C_{2v} symmetry. Besides the long-bridge hollow site, there are two facet sites along the close-packed direction in the fcc(110) and the hcp(10$\bar{1}$0) surfaces. One is the hcp(0001) facet hollow site (I) that contains one atom in the top layer and two atoms in the second layer; the other is the fcc(111) facet (labeled II) that contains two atoms in the top layer and one in the second layer along the close-packed direction. The fcc(110) and (111) surfaces are analogous to the hcp(10$\bar{1}$0) and (0001) surfaces with a slight difference in the interatomic spacing.

Table 2.2 lists the values of electronegativity (η), possible valences, and the atomic radius of representative elements of different electronic structures. The difference in electronegativity between atoms of two elements determines the nature of the bond between them. If the $\Delta\eta$ is sufficiently high (around 2), the bond is ionic; otherwise, it is covalent or polar covalent [1]. Normally, the atomic size of a noble ($4d$) metal is greater than that of a transition ($3d$) metal and the electronegativity of the noble metals is higher than that of transition metals. An atomic radius is not a constant but varies with the coordination number (CN) of this atom. Importantly, atomic radii change with alternation of valences. These basics play important roles in specifying the site of the adsorbate and the orientation of the tetrahedron bonds involving C, N, and O and therefore the patterns of observations for the chemisorbed surfaces.

2.1.3 Bonding Effects

Bond formation is a process in which valence electrons transport. This should have enormous effects on the surroundings by polarization and mass transportation. Alternation of atomic sizes will change the atomic distances and modify the surface morphology. Besides the well-known bonding states of metallic, covalent, ionic, and Van der Waals bonds in nature, polar covalent bonds, non-bonding lone pairs, antibonding dipoles, H-like bonds, and hydrocarbon-like bonds also exist.

Despite the well-known bonding events illustrated in Fig. 2.2a–h describes the formation of an ionic bond, non-bonding lone pairs, and their consequences on the wave functions of their atomic neighbors. The electronegative adsorbate or additive (smaller broken circle labeled *A*) interacts with the heavier host atoms (bigger broken circle labeled *B*) by either capturing electrons from the host *B* atom or polarizing the electrons of *B*. The polarization will raise the binding energy of the polarized electrons to the higher energy levels. Electron transport alters the atomic valences and atomic sizes of both the adsorbate *A* and the host *B*. For example, an oxygen atom changes its radius from 0.66 to 1.32 Å when the oxygen atom evolves into an O^{-2} ion. A copper atom alters its radius from 1.278 to 0.53 Å when the Cu atom becomes a Cu^{+} ion.

All the ions, whether positive or negative, and the non-bonding lone pairs are apt to polarize their neighbors, giving rise to the host dipoles with localized nature. Dipoles are formed with the expansion of atomic sizes and elevation of the DOS in energy. The production of the dipoles and the dipole–dipole interaction in the opposite direction will raise the system energy. It is therefore reasonable to term such an event as antibonding dipole formation—an extreme case of the Van der Waals bond interaction. Antibonding is a by-product of reaction, and it never forms between atoms of different electronegativities [4].

Non-bonding lone pairs meant that a pair of electrons of a specific atom occupies a directional bonding orbital of this atom. Lone-pair formation happens only to electronegative elements in the upper right part of the periodic table, such as

Table 2.2 Electronegativity, possible valences, and the *CN*-related atomic radius of typical elements (after Goldschmidt [2] and Pauling [1])

Element	C	N	O	Si	Co	Cu	Ag	Ru	Rh	Pd	V
Electronic structure	$2s^2p^2$	$2s^2p^3$	$2s^2p^4$	$3s^2p^2$	$3d^74s^2$	$3d^{10}4s^1$	$4d^{10}5s^1$	$4d^75s^1$	$4d^85s^1$	$4d^{10}5s^0$	$3d^34s^2$
η	2.5	3.0	3.5	1.9	1.9	1.9	1.9	2.2	2.2	2.2	1.6
R_{ion} (valence)	2.6 (−4)	1.71 (−3)	1.32 (−2)	0.41 (4)	0.82 (2)	0.53 (1)	1.00 (1)	–	–	–	–
R_m ($CN = 1$)	0.771	0.70/0.74	0.66/0.74	1.173	1.157	1.173	1.339	1.241	1.252	1.283	1.224
R_m ($CN = 12$)	0.914	0.88/0.92	–	1.316	1.252	1.276	1.442	1.336	1.342	1.373	1.338

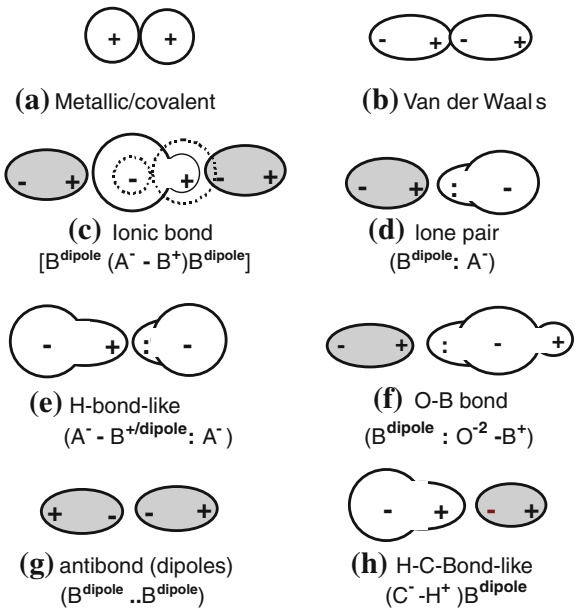

Fig. 2.2 The possible bond configurations and their consequences on the electron clouds of surrounding atoms (*shaded areas* stand for dipoles). **a** and **b** are the well-known bonding events. **c** Ionic bond formation alters atomic sizes (*broken circles*) and valences. **d** Non-bonding lone-pair formation (represented by ':') induces B^p. **e** H-like bond forms if $B^{+/p}$ replaces the $H^{+/p}$. **f** O–M bonds involve non-bonding lone pairs and bonding electron pairs. **g** Antibonding dipoles. **h** Hydrocarbon-like bonds can form by replacing H^+ with B^+, which also induces antibonding dipoles (reprinted with permission from [3])

nitrogen, oxygen, and fluorine when the $2s$, $2p_x$, $2p_y$ $2p_z$ orbitals of these elements are hybridized [5]. It is often the case that a fraction of the hybridized orbitals is occupied by shared electron pairs (bonding) and the remaining orbitals by the lone electron pairs (non-bonding) of the electronegative additives. The number of lone pairs of an adsorbate follows a '$4-n$' rule, and the n is the valence value of the adsorbate. For oxygen ($n = 2$), two lone pairs are present, while for nitrogen ($n = 3$), only one lone pair forms during the *sp*-orbital hybridization. The '$4-n$' rule holds for any elements in which the *sp* orbits hybridize. The lone pair requires an interaction with a *B* atom through polarization without any charge transport. The lone pair is actually not a bond but the weaker part of the hydrogen bond.

The classical hydrogen bond (O^{-2} –$H^{+/p}$:O^{-2}), known for over 50 years, plays an essential role in the structure and function of biologic molecules. The '–' and ':' represent the bonding pair and the non-bonding lone pair, respectively. Hydrogen bonds are responsible for the strength and elasticity of materials such as wood or a spider's web, molecular binding, as well as base pairing and folding in DNA. Hydrogen bonds are also responsible for the synthesis and transferring of protein signaling [6, 7].

The formation of the hydrogen bond is not due to the existence of hydrogen or oxygen but a consequence of the non-bonding lone pairs. If the lone-pair-induced B^p bonds further to an electronegative element *A*, then an H-like bond (O^{-2}–$B^{+/p}$:O^{-2}) forms. H-like bonding differs from the classical hydrogen bond simply in that the $B^{+/p}$ replaces the $H^{+/p}$ in the hydrogen bond (see Fig. 2.2e). If an atom of another electronegative element, such as C, replaces one of the oxygen ions, then the (C^{-4}–$B^{+/p}$:O^{-2}) configuration forms, which was specified as the anti-hydrogen bond [8]. This is also an H-like bond. Formation of such an H-like bond depends merely on the existence of the lone pair rather than the particular B elements involved. Hence, the H-like bond is more generally applicable though it is not often referred to as such. The same is true for the hydrocarbon-like bonds. The hydrocarbon bond is polar covalent in nature. The naked H^+ also polarizes and attracts electrons of its neighboring atoms. Hydrocarbon-like bond can form by replacing the H^+ with B^+. The B^+ is less electronegative than the carbon.

The production of non-bonding lone pairs, antibonding dipoles, H-like bonds, and the hydrocarbon-like bonds is often overlooked. However, these events indeed play crucial roles in determining the physical properties of a system that involves electronegative additives. Quite often, a system contains several kinds of chemical bonds, such as in graphite and in an oxide. Because of the sp^2-orbital hybridization of carbon, the Van der Waals bond dominates in the [0001] direction, while the stronger covalent bond dominates in the (0001) plane of the graphite. As is shown in Fig. 2.2f, g, O–B bond formation involves sharing pairs of electrons (bond), non-bonding lone pairs, and antibonding dipoles. The electronic environment surrounding an oxygen atom or a nitrogen atom is anisotropic.

From an energy point of view, bond formation lowers the system energy and stabilizes the system. Antibond dipole formation requires additional energy. Although it is energetically less favorable, the antibond can still form as a by-product of the events of bonding and non-bonding. Occupation of the orbitals by non-bonding electron lone pairs of an electronegative element, in principle, neither raises nor lowers the system energy with respect to the initially specific energy level of the isolated atoms of the electronegative element [4, 9, 10]. From the band structure point of view, the antibond-derived DOS (or polaron) should locate at energy above E_F or near to it due to the energy rise of the polarized electrons. The DOS features for bonding are located below the originally occupied levels of the electronegative element, while the DOS features of non-bonding lone pairs are located between those of the bond and those of the antibond. Hydrogen-like bond formation will stabilize the system as electrons transport from the high-energy antibonding states to the lower bonding states. Bond and antibond formations will produce holes below the E_F of the host material [11], which should be responsible for the transition from metal to semiconductor when a compound forms.

2.1.4 Surface Bond Contraction

Besides the well-known fact that an atom changes its radius when its valence alternates, both the ionic and metallic radii of an atom contract with reducing the *CN* of this atom. Goldschmidt [2] suggested that if an atom changes its *CN* from 12 to 8, 6, and 4, then the ionic radius would be reduced by 3, 4, and 12 % correspondingly. Pauling [1] also noted that the metallic radius contracts considerably with the reduction in the *CN* of the metal atom. One may extend the *CN*-imperfection-induced radius contraction to atoms at a solid surface or sites surrounding defects (such as point defects and stacking errors). It is understandable that the surface provides an ideal environment for *CN* reduction. Termination of the lattice periodicity in the surface normal direction reduces the *CN* of an atom at the surface. Such a *CN* reduction shortens the remaining bonds of the surface atom. It is essential to consider the *CN* effect on the Goldschmidt contraction for an ionic bond or a Pauling contraction for a metallic bond.

2.2 Chemical Bond: Tetrahedron Geometry

Extending the FH, H_2O, NH_3, and CH_4 molecular structures to a chemisorbed surface by replacing the H atom with the host atom of an arbitrary element B, one can construct the tetrahedron bond configuration, as illustrated in Fig. 2.3a for oxide instance. During the modeling, two factors are taken into consideration. Firstly, the atomic radius is not constant but varies with the changes in not only its atomic valence, but also its *CN*. Secondly, the *sp* orbits of oxygen hybridize and a quasi-tetrahedron forms. The bond angles and the bond lengths are not constant but vary within limits. Therefore, an oxygen atom can react with atoms, in any gaseous, liquid, or solid states of an arbitrary element B through two bonding electron pairs and two non-bonding lone pairs.

Oxygen atom has initially six electrons in the 2*s* and 2*p* orbits and then captures two more electrons from each of its *B* neighbors. The eight electrons fully occupy the 2*s* and 2*p* levels of an oxygen atom that hybridizes its *sp* orbits then to form four directional orbits. The eight electrons repopulate in the four directional orbitals with two electron pairs shared between O and B. The remaining two orbits are occupied by the lone electron pairs of oxygen.

In a bonding orbit, the extent of electron sharing, or the nature of the bond, depends on the difference in electronegativity (η) between the oxygen and element *B*. Due to the high η value (see Table 2.2), oxygen catches an electron from *B* (labeled 1 and 2 in Fig. 2.3a) to form the ionic bond with Goldschmidt contraction at the surface. Formation of the non-bonding lone pairs, however, is independent of the nature of element B. The lone pairs polarize atom *B* (labeled 3 in Fig. 2.3a), and the *B* atom becomes a B^p dipole with associated expansion of size and elevation of energy of the polarized electrons that occupy the antibonding energy levels.

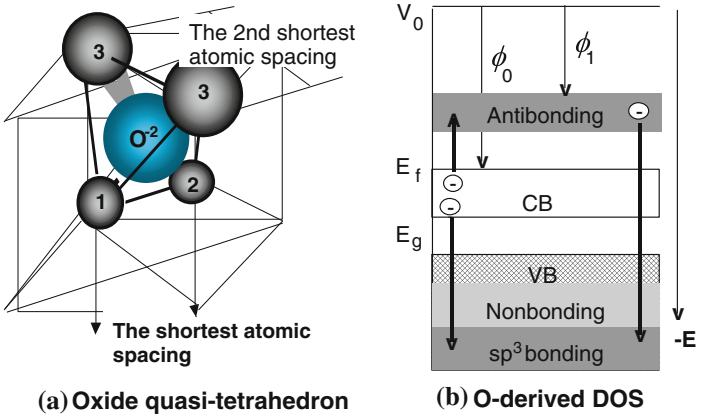

Fig. 2.3 **a** the primary oxide quasi-tetrahedron and, **b** the corresponding DOS features of bonding, non-bonding, antibonding, and electronic holes [12]. Each of the two ions, 1 and 2, donates one electron to the central oxygen to form ionic bonds with Goldschmidt contraction. Atoms labeled 3 are the lone-pair-induced metal dipoles with expansion of sizes and elevation of energy states. Due to the repulsion between the electron pairs, the angle BA33 is greater than 109.5° and the angle BA12 is smaller than 104.5°. *Arrows* in (**b**) represent the process of charge transportation. The *arrow* from the antibonding sub-band to the bond states corresponds to the process of H-like bond formation (reprinted with permission from [3])

In an oxide tetrahedron, the plane (3O3) composed of the lone pairs and the oxygen nucleus should be ideally perpendicular to the plane (1O2) that consists of two bonding orbits. The distance (1–2) between the two B^+ ions and the spacing (3–3) between the B^p and B^p match closely the first and second shortest atomic spacings at a surface, which involves two atomic layers. The B^p tends to locate at the open end of a surface due to the strong repulsion between the dipoles. The B_2O primary tetrahedron is not a standard one, but it is distorted due to the following effects: (1) the difference in repulsion between the occupied orbits varies the bond angles [BAij (angle ∠iOj), where $i, j = 1, 2, 3$ correspond to the atoms as labeled; BA12 $\leq$ 104.5°, BA33 $>$ 109.5°] and (2) the difference in *CN* of atoms at different sites adjusts the bond length [BLi $= (R_M^+ + R_O^{-2}) \times (1-C_i)$, where $i = 1$, 2; C_i are the effective bond contracting factors]. The length of BL3 and the angle BA33 vary with the coordination circumstances in a real system. The bonding environment for an oxygen atom is anisotropic at the atomic scale.

The formation of tetrahedrons dislocates the *B* atoms collectively in the otherwise regular lattice sites. Moreover, an oxygen atom always seeks four neighbors to form a stable quasi-tetrahedron. The expansion of atomic radius and the energy rise of the dipole electrons are responsible for the protrusions in the STM images and the reduction in the local work function. The localized dipole electrons are also responsible for the non-Ohmic rectification at the surface, even though the local work function reduces significantly. The strong localization of dipole electrons at the surface increases the surface contact resistance because

these electrons cannot move easily. The oxygen adsorption affects the STM current predominantly by polarizing metal electrons, because of antibonding dipole formation [13–15].

At the initial stage of oxidation, the oxygen molecule dissociates and the oxygen atom interacts with the host atoms through a single bond. The O^{-1} chooses a specific site where the O^{-1} bonds directly to one of its neighbors and polarizes the rest. For the transition metals, such as Cu and Co, of lower electronegativity ($\eta < 2$) and smaller atomic radius (<1.3 Å), the oxygen atom often bonds to an atom at the surface first. For noble metals, such as Ru and Rh, of higher electronegativity ($\eta > 2$) and larger atomic radius (>1.3 Å), the oxygen atom tends to sink into the hollow site and bonds to the atom underneath the first atomic layer. The ordering of bond formation leads to different patterns of reconstruction. The O^{-1} also polarizes other neighbors and pushes the B^p at the surface radially outward from the adsorbate. Because of oxide tetrahedron formation with lone-pair non-bonding and dipole antibonding, the electronic structure surrounding a certain atom varies from site to site.

2.3 Energy Band: Valence Density of States

The formation of bonds, non-bonding lone pairs, and antibonding dipoles as well as the H-like bonds generates corresponding features adding to the DOS of the valence band and above of the host, as illustrated in Fig. 2.3b. Arrows represent the kinetic processes of electron transportation. Initially, energy states below the E_F of a metal are fully occupied in the ideal case at $T = 0$. The work function, ϕ_0, Fermi energy, E_F, and the vacuum level, E_0, follow the simple relation: $E_0 = \phi_0 + E_F$. For Cu, as an example, $E_0 = 12.04$ eV, $\phi_0 = 5.0$ eV, and $E_F = 7.04$ eV. The Cu-3*d* band locates at energies range over from −2.0 to −5.0 eV below E_F. The oxygen 2*p* states are around −5.5 eV with respect to E_F for Cu. At the initial stage of reaction, an electron from a metal is transported from its outermost shell to the unoccupied 2*p* orbit of the oxygen, which produces a hole in the outermost shell of the metal. The O^{-1} polarizes its rest neighbors to form a polaron, as a result. This first stage creates additional DOS features of bonding ($\ll E_F$), holes ($\leq E_F$), and antibonding dipoles ($\geq E_F$).

With the full occupancy of the *p*-orbit of oxygen, the *sp* orbits of the O^{-2} hybridize, which brings about four additional DOS features, as illustrated in Fig. 2.3b:

- Electronic vacancies pertaining to the host are produced right below E_F, generating a gap between the conduction band and the valence band of a metal. The electron transportation can also expand the original bandgap of a semiconductor from E_{G0} to E_{G1}.
- The non-bonding states of O^{-2} locate below E_F without apparent energy change, in principle, compared with the 2*p* level of an isolated atom of oxygen [9].

- The bonding states are close to the originally occupied $2p$ level of the isolated oxygen.
- The antibonding (lone-pair-induced dipole) states are located above E_F or near to it. The oxygen-induced dipole reduces the work function from ϕ_0 to ϕ_1.
- Upon being overdosed with oxygen, H-like bonds form at the surface. The overdosed oxygen gets electrons from the dipoles, and the B^p becomes $B^{+/p}$. The arrow from the antibonding states above E_F to the deeper bonding sub-band represents the process of H-like bond formation. Apparently, this process lowers the system energy and increases the work function.

The hole production and the lone-pair production are independent but simultaneous, which result in the joint DOS features below E_F. If the products of both processes are compatible in quantity, the joint DOS features derived by the two processes may not be easily identified. The hole production is due to two mechanisms: bonding and antibonding. For the Cu example, the $4s$ electrons (in the conduction band, CB) either contribute to oxygen for the bonding or jump up to the outer empty shell (Cu $4p$, for example) for the antibonding dipole. Such bonding and antibonding processes empty the states just below E_F, which result in the Cu oxide being a semiconductor with a known bandgap ranging from 1.2 to 1.5 eV [16, 17].

STS and VLEED revealed that the states of antibonding of the O–Cu system range over 1.3 ± 0.5 eV above the E_F and the non-bonding states -2.1 ± 0.7 eV below. Angular resolved inverse PES [18] detected that the features of empty states at +2.0 eV decrease with increasing oxygen coverage on the Cu(110) surface. The PEEM studies of O–Pt surfaces [19–22] have detected the conversion of the dark islands, in the scale of 10^2 μm, into very bright ones with work functions ~ 1.2 eV lower than that of the clean Pt surface. The bonding states are around -5.5 eV below E_F, which is shifted slightly toward an energy level lower than the $2p$ level of the oxygen because the hybrid bond lowers the system energy. Most strikingly, all the oxygen-derived DOS features are strongly localized in real space.

Non-bonding lone pairs and antibonding dipoles are generated in a reaction with sp^3-orbit hybridization being involved, such as in the processes of

$$\begin{aligned} NH_3 &\rightarrow 3H^+ - N^{3-}\left(:H^P\right) \\ H_2O &\rightarrow 2H^+ - O^{2-}\left(:2H^P\right) \\ HF &\rightarrow H^+ - F^-\left(:3H^P\right) \end{aligned}$$

Usually, the parts in the brackets are omitted in formulating reactions because they share no charges with the electron acceptors. Under UV irradiation or thermal excitation, the hybrid sp^3-orbit can be dehybridized, and the lone pairs and dipoles are removed accordingly.

Figure 2.4 illustrates the residual DOS of N- and O-chemisorbed metals and semiconductors. Likewise, a nitrogen atom needs three electrons for sharing and

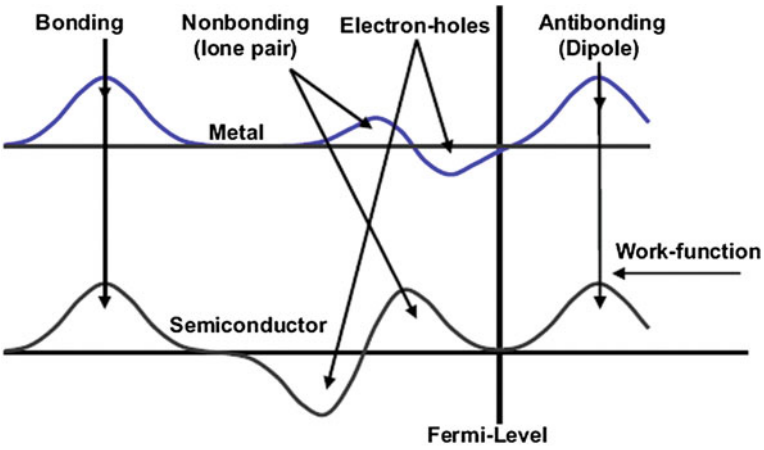

Fig. 2.4 N, O, and F chemisorption modified valence DOS for a metal and a semiconductor with four excessive DOS features: bonding ($\ll E_F$), lone pairs ($<E_F$), electron holes ($<E_F$), and dipoles ($>E_F$). The three DOS features close to the E_F are often overlooked, yet they are crucial to the performance of a compound (reprinted with permission from [3])

generates one lone pair. Similarly, an F atom forms a tetrahedron with three lone pairs. In additional to the weak interactions with energies of $\sim$50 meV [3], these lone pairs polarize the neighboring atoms instead causing their change to dipoles. Strikingly, the manner of electronic distribution, bond type, bond length, and bond energy surrounding the central O or N atom in the tetrahedron is anisotropic.

In semiconductor compounds, the holes form at the upper edge of the valence band, which expand the semiconductor's bandgap further and turn a semiconductor into an insulator. In metallic compounds, the holes are produced at the Fermi surface and hence causing the formation of a bandgap. This is the reason for the metallic compound's loss of conductivity to become either a semiconductor or an insulator. Non-bonding states are situated in the bandgap to form impurity states close to Fermi surface, while antibonding states are situated above the Fermi energy. The production of dipoles will shift the surface potential barrier outwardly with high saturation [23], opposing to the effect of the charged ions. The former can be observed using STM as protrusions, while the latter depressions. The orientation of such a tetrahedron in a bulk is also subject to its coordination environment [24]. The difference between N, O, and F is in the structural symmetry and the number of lone pairs in one tetrahedron.

The weak interactions contribute insignificantly to the Hamiltonian or the atomic cohesive energy. These electrons add, however, impurity states near Fermi energy, which neither follow the regular dispersion relations nor occupy the allowed states of the valence band and below. They are located right in the energy scope of STM/S. The lone-pair and dipole interactions not only act as the most important function groups in the biologic and organic molecules but also play an important role in the inorganic compounds.

2.4 Surface Potential Barrier: Morphology

The SPB experienced by LEED incident electrons traversing the surface region contains two parts [25]:

$$\begin{aligned} V(r,E) &= \mathrm{Re}V(r) + \mathrm{iIm}V(r,E) \\ &= \mathrm{Re}V(r) + \mathrm{iIm}[V(r) \times V(E)] \end{aligned} \tag{2.1}$$

The shape and the saturation degree of the SPB depend on the surface atomic valence states [26], but the height of the SPB approaches to the muffin-tin inner potential constant of atoms inside the solid, V_0 [27]. The real (elastic) and imaginary (inelastic) parts of the SPB take the following forms [27, 28]:

$$\mathrm{Re}V(z) = \begin{cases} \frac{-V_0}{1+A\exp[-B(z-z_0)]}, & \mathrm{z} \geq \mathrm{z}_0(\text{a psuedo-Fermi-z function}) \\ \frac{1-\exp[\lambda(z-z_0)]}{4(z-z_0)}, & \mathrm{z} < \mathrm{z}_0(\text{the classical image potential}) \end{cases}$$

$$\begin{aligned} \mathrm{Im}V(z,E) &= \mathrm{Im}[V(z) \times V(E)] \\ &= \gamma \times \rho(z) \times \exp\left[\frac{E-\phi(E)}{\delta}\right] \\ &= \frac{\gamma \times \exp\left[\frac{E-\phi(E)}{\delta}\right]}{1 + \exp\left[-\frac{z-z_1}{\alpha}\right]} \end{aligned}$$

where A, B, γ, and δ are constants. α and λ describe the degree of saturation. z_0 is the origin of the image plane inside which electron is located. $\phi(E) = E_0 - E_\mathrm{F}$, the energy-dependent local $\phi(E)$ depends on the density of states $\rho(E)$. The $\nabla^2[\mathrm{Re}V(z)] = -\rho(z) \propto \mathrm{Im}V(z)$ describes the spatial distribution of charges. The terms $z_1(z_0)$ ($\rho(z_1) = 0.5\rho_\mathrm{bulk}$) and $\alpha(z_0)$ (saturation degree) involved in the Fermi z function describe the spatial distribution of electrons contributing to the damping of incident beams. The spatial integration of $\rho(z)$ from a position inside the crystal to infinitely far away from the surface gives the local DOS ($n(x, y)$). Therefore, $\phi_L(E)$ can extend to cover situations that are E dependent and to large surface areas over which the LEED method integrates (Fig. 2.5).

The real part, $\mathrm{Re}V(r)$, describes the elastic scattering of the incident electron beam. Integration of the $\mathrm{Re}V(r)$ along the moving path of the electron beam determines the phase shift of the electron beam in diffraction. The imaginary part, $\mathrm{Im}V(r)$, describes the spatial decay of the incident beam. $\mathrm{Im}V(E)$ represents the joint effects of all the dissipative processes including excitation of phonons, photons, and single electron as well as plasmon excitation. Plasmon excitation occurs at energy much higher than E_F (normally $\sim$15 eV above E_F). Excitation of phonon and photon requires energy smaller than the work function. Single-electron excitation occurs at any beam energy that is greater than the work function and in the space occupied by electrons. The spatial distribution of electrons is described by $\rho(r)$ (charge density) that is related to the inelastic damping potential, $\mathrm{Im}V(r)$. An $\mathrm{Im}V(z, E)$ can be defined

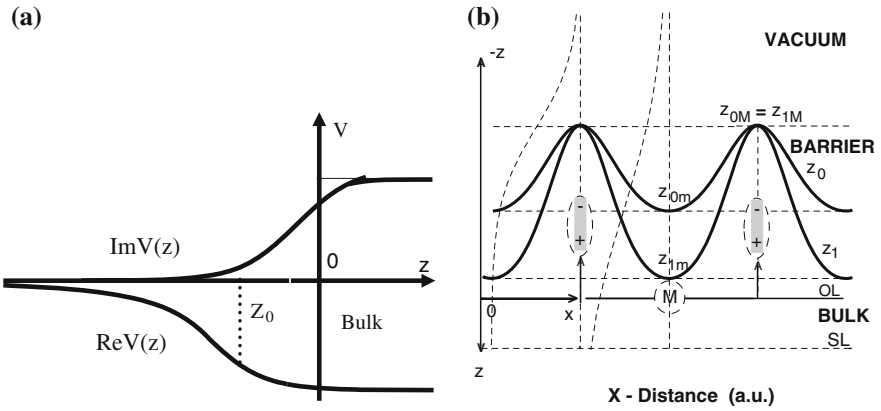

Fig. 2.5 **a** The real (elastic) and imaginary (damping) parts of the SPB with z-axis directed into the crystal, and z_0 is the origin for the image plane. The imaginary part describes surface charge distribution and saturation, which correspond to the surface morphology. The elastic part is related to the path and phase shift of diffracted electron beams in LEED measurements. **b** The SPB correlates STM surface morphology. At dipole site, the SPB origin shifts out of the surface with high saturation, while at vacancy or the ionic site, the SPB shifts inward and less saturated (reprinted with permission from [3])

to include the damping effects that occurs in the electron-occupied space (Fermi z decay) and that takes place at incident beam energy being greater than the work function, which depends on the occupied DOS [29].

The Re$V(r)$ correlates with the Im$V(r)$ through the Poisson equation:

$$\nabla^2[\mathrm{Re}V(r)] = -\rho(r); \text{ and, } \mathrm{Im}V(r) \propto \rho(r)$$

The gradient of the Re$V(r)$ relates to the intensity of the electric field $\varepsilon(r)$: $\nabla[\mathrm{Re}V(r)] = -\varepsilon(r)$. If $\rho(r) = 0$, then the Re$V(r)$ corresponds to a conservative field in which the moving electrons will suffer no energy loss and the spatial variation in the inelastic potential Im$V(r) \propto \rho(r) = 0$. The Re$V(z)$ transforms at $z = z_0$ from the pseudo-Fermi z function to the $1/(z-z_0)$-dominated classical image potential. Therefore,

$$\nabla^2[\mathrm{Re}V(z_0)] = -\rho(z_0) = 0.$$

The origin of the image plane, z_0, acts as the boundary of the surface region occupied by electrons. If z_0 varies with the surface coordinates, then the $z_0(x, y)$ provides a contour of the spatial electron distribution, which should be similar to that plotted using STM imaging [29].

At the dipole site, $z_{1M} \approx z_{0M} = -3.425$, $\alpha \approx \lambda^{-1}$, while in the atomic vacancy or ion positions, $z_{1m} \ll z_{0m} = 1.75$ Bohr radii due to the strong localization of electrons at the surface. The SPB increases its degree of saturation with the outward shift of the image plane z_0. This means that formation of metal dipoles shifts the electron clouds outwardly and enhances the density of the shifted electronic clouds.

2.5 Summary

The H_2O-, NH_3-, and FH-like molecular structures and the concept of *CN*-imperfection-induced bond contraction can be extended to the chemisorption of a solid surface. This leads to the framework of tetrahedral bond formation and its effects on the valence DOS and the surface potential barrier, as well as their interdependence:

- O, N, C, and F can interact with atoms of an arbitrary element B to form a tetrahedron with bonding and non-bonding states, as well as antibonding dipoles due to polarization.
- Chemisorption of electronegative additives derives four additional DOS features that add to the valence band and above of the host. These features of bonding, non-bonding, antibonding, and electron holes are strongly localized.
- The SPB parameters are correlated with the image plane (z_0) corresponding to the boundary of the surface region occupied by electrons, which describe the STM imaging features.
- The bond geometry, atomic valence values, valence DOS, and the SPB are interdependent. One may need to pay equal attention to these categories in dealing with surface chemisorption. This way of thinking will amplify immensely the physics behind observations and enhance the capacity of available instrumentation.
- Some important yet often overlooked events, such as non-bonding lone pairs, antibonding dipoles, H-like bond, and surface bond contraction, are crucial to practical applications.

References

1. L. Pauling, Atomic radii and interatomic distances in metals. J. Am. Chem. Soc. **69**(3), 542–553 (1947)
2. V.M. Goldschmidt, Crystal structure and chemical correlation. Ber. Deut. Chem. Ges. **60**, 1263–1296 (1927)
3. C.Q. Sun, Oxidation electronics: bond-band-barrier correlation and its applications. Prog. Mater. Sci. **48**(6), 521–685 (2003)
4. S.R. Morrison, *The Chemical Physics of Surfaces* (Plenum press, NY and London, 1977)
5. C.W. Keenan, D.C. Kleinfelter, J.H. Wood, *General College Chemistry* (Harper and Row Publishers, New York, 1979)
6. W.G. Han, C.T. Zhang, A theory of nonlinear stretch vibrations of hydrogen-bonds. J. Phys.: Condens. Matter **3**(1), 27–35 (1991)
7. R.H. Crabtree, Chemistry—A new type of hydrogen bond. Science **282**(5396), 2000–2001 (1998)
8. P. Hobza, Z. Havlas, The fluoroform center dot center dot center dot ethylene oxide complex exhibits a C–H center dot center dot center dot O anti-hydrogen bond. Chem. Phys. Lett. **303**(3–4), 447–452 (1999)
9. J.M.D. Coey, H. Sun, Improved magnetic-properties by treatment of iron-based rare-earth intermetallic compounds in ammonia. J. Magn. Magn. Mater. **87**(3), L251–L254 (1990)

10. P.W. Atkins, *Physical Chemistry* (Oxford University Press, Oxford, 1990)
11. C.Q. Sun, C.L. Bai, A model of bonding between oxygen and metal surfaces. J. Phys. Chem. Solids **58**(6), 903–912 (1997)
12. C.Q. Sun, What effects in nature the two-phase on the O–Cu(001)? Mod. Phys. Lett. B **11**(2–3), 81–86 (1997)
13. N.D. Lang, Apparent barrier height in scanning tunneling microscopy. Phys. Rev. B **37**(17), 10395–10398 (1988)
14. N.D. Lang, Small adsorbate dipole-moments need not imply small charge transfers. Surf. Sci. **127**(2), L118–L122 (1983)
15. N.D. Lang, in *Scanning Tunneling Microscopy III*. Springer Series in Surf. Sci., Vol. 29, ed. by R. Wiesendanger, H.J. Güntherodt (Springer, Berlin, 1993)
16. J. Ghijsen, L.H. Tjeng, J. Vanelp, H. Eskes, J. Westerink, G.A. Sawatzky, M.T. Czyzyk, Electronic-structure of Cu2O and CuO. Phys. Rev. B **38**(16), 11322–11330 (1988)
17. F. Marabelli, G.B. Parravicini, F. Salghettidrioli, Optical gap of CuO. Phys. Rev. B **52**(3), 1433–1436 (1995)
18. A. Goldmann, M. Donath, W. Altmann, V. Dose, Momentum-resolved inverse photoemission-study of nickel surfaces. Phys. Rev. B **32**(2), 837–850 (1985)
19. H.H. Rotermund, Investigation of dynamic processes in adsorbed layers by photoemission electron-microscopy (PEEM). Surf. Sci. **283**(1–3), 87–100 (1993)
20. H.H. Rotermund, J. Lauterbach, G. Haas, The formation of subsurface oxygen on Pt(100). Appl. Phys. A-Mater. Sci. Process. **57**(6), 507–511 (1993)
21. J. Lauterbach, H.H. Rotermund, Spatiotemporal pattern-formation during the catalytic CO-oxidation on Pt (100). Surf. Sci. **311**(1–2), 231–246 (1994)
22. J. Lauterbach, K. Asakura, H.H. Rotermund, Subsurface oxygen on Pt (100): kinetics of the transition from chemisorbed to subsurface state and its reaction with CO, H_2 and O_2. Surf. Sci. **313**(1–2), 52–63 (1994)
23. C.Q. Sun, O-Cu (001): I. Binding the signatures of LEED, STM and PES in a bond-forming way. Surf. Rev. Lett. **8**(3–4), 367–402 (2001)
24. C.Q. Sun, Electronic process of Cu (Ag, V, Rh)(001) surface oxidation: atomic valence evolution and bonding kinetics. Appl. Surf. Sci. **246**(1–3), 6–13 (2005)
25. J.B. Pendry, *Low Energy Electron Diffraction: The Theory and its Application to the Determination of Surface Structure* (Academic Press, London, 1974)
26. C.Q. Sun, Spectral sensitivity of the VLEED to the bonding geometry and the potential barrier of the O-Cu (001) surface. Vacuum **48**(5), 491–498 (1997)
27. C.Q. Sun, C.L. Bai, Modelling of non-uniform electrical potential barriers for metal surfaces with chemisorbed oxygen. J. Phys.: Condens. Matter **9**(27), 5823–5836 (1997)
28. R.O. Jones, P.J. Jennings, O. Jepsen, Surface-barrier in metals: a new model with application to W(001). Phys. Rev. B **29**(12), 6474–6480 (1984)
29. C.Q. Sun, S. Li, B.K. Tay, X.W. Sun, S.P. Lau, Solution certainty in the Cu (110)-(2×1)-2O(2-) surface crystallography. Int. J. Mod. Phys. B **16**(1–2), 71–78 (2002)

http://www.springer.com/978-981-4585-20-0

Relaxation of the Chemical Bond
Skin Chemisorption Size Matter ZTP Mechanics H2O Myths
Sun, C.Q.
2014, XXXII, 807 p. 258 illus., 182 illus. in color.,
Hardcover
ISBN: 978-981-4585-20-0